Autoheterodyne Characterization of Narrow-Band Photon Pairs

Vindhiya Prakash,[1,*] Aleksandra Sierant,[2] and Morgan W. Mitchell[1,3,†]
[1]ICFO—Institut de Ciències Fotòniques, The Barcelona Institute of Science and Technology, 08860 Castelldefels (Barcelona), Spain
[2]Institute of Physics, Jagiellonian University in Kraków, Łojasiewicza 11, 30-348 Kraków, Poland
[3]ICREA—Institució Catalana de Recerca i Estudis Avançats, 08010 Barcelona, Spain

(Received 11 January 2021; accepted 10 June 2021; published 19 July 2021)

We describe a technique to measure photon pair joint spectra by detecting the time-correlation beat note when nondegenerate photon pairs interfere at a beam splitter. The technique implements a temporal analog of the Ghosh-Mandel effect with one photon counter and a time-resolved Hong-Ou-Mandel interference with two. It is well suited to characterize pairs of photons, each of which can interact with a single atomic species, as required to study recently predicted photon-photon interaction in subwavelength atomic arrays. With this technique, we characterize photon pairs from cavity-enhanced parametric down-conversion with a bandwidth ≈ 5 MHz and frequency separation of ~ 200 MHz near the D_1 line of atomic Rb.

DOI: 10.1103/PhysRevLett.127.043601

Spontaneous parametric down-conversion (SPDC) is a ubiquitous technique in photonic quantum technology, where it is used to generate entangled photons with tailored spectral, spatial, and polarization properties [1]. The frequency correlations of SPDC photon pairs, including time-frequency entanglement, are of particular importance. In some applications these correlations are used to encode quantum information [2,3]. In others, the frequency correlations are an undesired side channel that reduces nonclassical interference [4]. These correlations are revealed through analysis of the joint spectral amplitude (JSA) or joint spectral intensity (JSI) of the down-converted photon pair.

In broadband SPDC applications, it is possible to directly measure the JSI using monochromators or other passive filters [5,6]. Techniques such as Fourier transform spectroscopy using Mach Zehnder interferometers [7] and temporal magnification of photons with a time lens [8] have also been used. Nonclassical interference can also be a tool to characterize nonclassical frequency correlations; the Hong-Ou-Mandel (HOM) [9] interference visibility has been used to characterize broadband photon pairs from a single source [3,6,10] and from different sources [11,12].

Photon pairs with ~MHz bandwidths are important for applications in quantum information [13] where material systems such as atoms or ions serve as storage or processing units [14,15]. For example, subwavelength arrays of neutral atoms support subradiant states [16] that can exhibit topological protection [17] and unprecedented optical properties [18]. Strong photon-photon interactions [19] that could be harnessed for photonic quantum-information processing, and photonic bound states [20,21] are predicted in such arrays. Exploring this physics motivates nonclassical light sources in which both photons are resonant to an atomic transition [22]. Applications in quantum networking, e.g., entanglement swapping with memory-compatible photons, will require pure, indistinguishable, narrow-band photons [23].

Such narrow-band photon pairs are not easily measured by passive frequency-domain techniques, because of the very high optical frequency resolution it would require. In such a two-photon Fock state, first-order interference vanishes, producing no observable beat note [24]. One alternative is stimulated parametric down-conversion [25], in which laser photons are used to seed the down-conversion and map the difference frequencies generated vs those suppressed [22,26]. This technique has potential for use in tomography of the JSA [27], but requires an additional well-characterized laser source and careful matching of spatial modes.

Here we present a simpler and more efficient alternative, a time-domain characterization of the two-photon state using nonclassical interference. The JSI is a two-dimensional function, while the HOM interference visibility is a scalar observable. Thus a characterization of the JSI even along a single dimension requires many HOM visibility measurements under changing experimental conditions, such as a changing path length [28,29]. In contrast, the Ghosh and Mandel experiment [30] (GM), which measured the spatial interference pattern produced by photons of unequal momentum, showed how a correlation spectrum can be acquired with a single experimental condition. This motivates us to look for techniques that give more direct and more efficient access to the frequency correlations of interest. Our proposals for narrow-band photon pair characterization, are extensions of the HOM and GM interference effects.

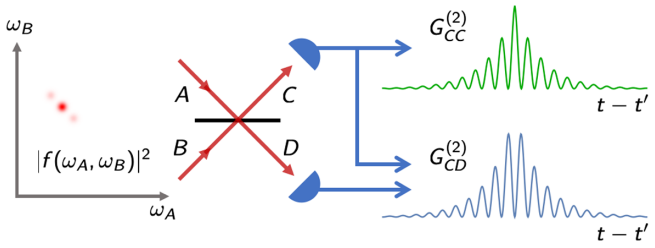

FIG. 1. Principle of the method. Two photons, one in mode A and one in mode B, with joint spectral amplitude $f(\omega_A,\omega_B)$, illustrated in the left graph (color density indicates square magnitude), meet at a 50:50 BS and are detected in modes C and D. Single-photon-sensitive detectors register the photon arrival times. The correlation functions $G^{(2)}_{C,C}(t,t')$, $G^{(2)}_{D,D}(t,t')$, and $G^{(2)}_{C,D}(t,t')$ oscillate with $t-t'$, revealing the distribution of $\omega_A-\omega_B$.

The principle of the method is illustrated in Fig. 1. Narrow-band photon pairs with the photons of each pair matched in polarization and spatial profile but with unequal frequency, are injected, one into port A and the other into port B of a 50/50 beam splitter (BS). Single-photon-sensitive detectors register photons leaving the BS by ports C and D, and time-tagging electronics record the arrival times. Many events are accumulated, and the second order correlation functions $G^{(2)}_{\kappa,\mu}(t,t')$, $\kappa,\mu\in\{C,D\}$ are calculated. Information about the JSA can then be inferred from the $G^{(2)}$ functions. We refer to this method as *autoheterodyne characterization* (AHC), not to be confused with the single-photon self-heterodyne technique [31].

When photons of different frequency meet at a BS, their arrival-time distribution becomes modulated at the difference of their frequencies. This can be understood as follows: a detection at C and D with zero time delay, i.e., $t=t'$, can happen by two channels in configuration space: either reflection of both photons or transmission of both photons. The amplitudes for these channels sum to zero, due to phase factors in the transmission and reflection processes. The resulting vanishing of $G^{(2)}_{C,D}(t,t)$ and the corresponding increase of $G^{(2)}_{C,C}(t,t)$ and $G^{(2)}_{D,D}(t,t)$ is the well-known HOM effect [9]. For unequal detection times, one must also consider the phase factors $\exp[-i\omega_A t-i\omega_B t']$ and $\exp[-i\omega_A t'-i\omega_B t]$ that apply to the two-reflection and two-transmission channels, respectively. The relative phase $(\omega_A-\omega_B)(t-t')$ between the channels then induces an oscillation of the $G^{(2)}$ correlations at the difference frequency $\omega_A-\omega_B$. We refer to this nonclassical interference between distinguishable photons as the nondegenerate HOM effect. Small frequency differences between the photons manifest as long-period oscillations in the relative arrival time distribution, which are technologically convenient to detect.

The effect can be easily calculated. For a two-photon input state $|\psi\rangle$ with JSA $f(\omega_A,\omega_B)$,

$$|\psi\rangle=\int d\omega_A d\omega_B f(\omega_A,\omega_B)\hat{a}^\dagger_A(\omega_A)\hat{a}^\dagger_B(\omega_B)|0\rangle. \quad (1)$$

The un-normalized correlation functions are $G^{(2)}_{\alpha,\beta}(t,t')\equiv|\langle 0|\hat{E}^{(+)}_\alpha(t)\hat{E}^{(+)}_\beta(t')|\psi\rangle|^2$, $\alpha,\beta\in\{A,B,C,D\}$, where the field operators are $\hat{E}^{(+)}_\alpha(t)\propto\int d\omega\hat{a}_\alpha(\omega)\exp[-i\omega t]$ and $\hat{a}_\alpha$ is an annihilation operator. Because of the beam splitter, the output fields are $\hat{E}^{(+)}_{C/D}(t)\propto\hat{E}^{(+)}_A(t)\pm\hat{E}^{(+)}_B(t)$. A straightforward calculation finds

$$G^{(2)}_{\kappa,\mu}(t,t')\propto\left|\int d^2\omega f(\vec{\omega})e^{-i\frac{\omega_+ t_+}{2}}\mathrm{osc}(\omega_- t_-/2)\right|^2, \quad (2)$$

where $\omega_\pm\equiv\omega_A\pm\omega_B$, $t_\pm\equiv t\pm t'$ and the integral is taken over ω_A, ω_B or, equivalently, over ω_+, ω_-, with $\vec{\omega}$ being the corresponding parametrization of f and $\mathrm{osc}\,\theta=(1/\sqrt{2})\cos\theta$ if $\kappa,\mu=C,C$ or D,D and $i\sin\theta$ otherwise. This describes a Fourier transform of the JSA along the $\omega_\pm$ coordinates. When the two-photon state is produced by SPDC, and pumped by a broadband pump with field $E_p(t)=\int d\omega_p\alpha(\omega_p)e^{-i\omega_p t}$, $f\propto\int d\omega_p\alpha(\omega_p)\delta(\omega_p-\omega_+)\times g(\omega_-,\omega_+)\propto\alpha(\omega_+)g(\omega_-,\omega_+)$. When the variation of the crystal phase matching function over the pump bandwidth can be neglected, g becomes independent of ω_+ and the JSA factorizes as $f\propto\alpha(\omega_+)g(\omega_-)$. The $G^{(2)}$ then gives the sine or cosine power spectrum of $g(\omega_-)$ in the t_- dimension and also gives the Fourier transformed spectrum of $\alpha(\omega_+)$ via the t_+ dimension [24]. For a monochromatic pump $\alpha(\omega_+)\to\delta(\omega_+-\omega_p)$, such that $f\propto\delta(\omega_+-\omega_p)g(\omega_-)$ and $G^{(2)}$ depends only on t_-. In what follows we study the narrow-band, cw-pump case. The use of AHC in the pulsed scenario and to obtain measures such as entanglement entropy, state purity and Schmidt number [32] is discussed in the Supplemental Material [24].

We note that this technique implements a variant of the GM effect [30]. In GM, photon pairs with unequal transverse momenta k_s, k_i are observed to produce a spatial autocorrelation function $G^{(2)}(x-x')$ that is maximum for $x-x'=0$ and modulated with momentum k_s-k_i. The temporal modulation of $G^{(2)}_{C,C}$ or $G^{(2)}_{D,D}$, which describes the correlations of photon pairs with unequal frequencies ω_A, ω_B in a single output channel, is the temporal analog of GM. We refer to this as the temporal Ghosh-Mandel effect. By conservation of probability at the BS, the GM and HOM signals must add to give $G^{(2)}_{A,B}(t,t')$, as illustrated in Fig. 1. As a result, the two methods give very similar information about the JSA.

To demonstrate this experimentally, we use photon pairs from a cavity-enhanced SPDC (CE-SPDC) source pumped by a single-frequency laser. The experimental setup is shown schematically in Fig. 2. Photon pairs are produced by a narrow-band CE-SPDC source, described in detail in

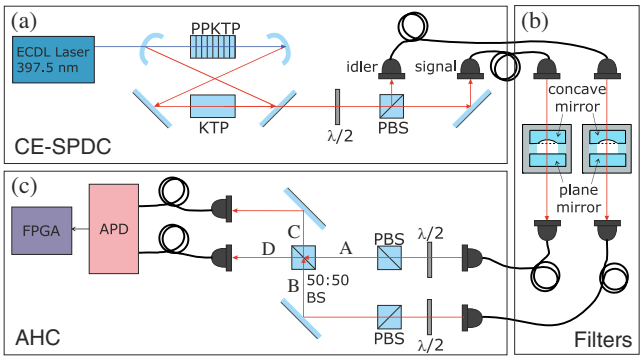

FIG. 2. Schematic of setup for generation and characterization of narrow-band photon pairs. (a) CE-SPDC source, consisting of a bow-tie cavity containing an ECDL-pumped SPDC crystal (PPKTP) and a second crystal (KTP). Photon pairs are separated by polarization. (b) Tunable FP filters are used to select desired "teeth" from the comb of CE-SPDC output modes. (c) Autoheterodyne characterization. The photons are set to the same polarization, interfered on a beam splitter (BS), detected using avalanche photodiodes and time-tagged with an FPGA. Polarizing beam splitter (PBS).

Ref. [22]. A pump laser at 397.5 nm with full width half-maximum (FWHM) linewidth ≈ 2 MHz pumps a type-II periodically poled potassium titanyl phosphate (PPKTP) crystal to produce photon pairs of orthogonal linear polarization. The cavity mode structure, with signal and idler free-spectral range (FSR_s and FSR_i) ≈ 500 MHz and FWHM linewidth $\gamma = 2\pi \times 7.6$ MHz for both H [signal (s)] and V [idler (i)] polarizations, shapes the output spectrum by the Purcell effect. Birefringent crystals in the SPDC cavity produce a mismatch of $\Delta\mathrm{FSR} = 3.5$ MHz in the FSRs of the signal and idler modes. This reduces the number of modes at the output to 3 clusters of 4 modes each for a down-conversion crystal bandwidth of 150 GHz as shown in Ref. [22]. The contribution of unwanted modes is blocked by a pair of tunable Fabry-Perot (FP) filters with linewidth $\gamma_f = 2\pi \times 97$ MHz and $\mathrm{FSR}_f = 39$ GHz.

To perform AHC of the CE-SPDC source, the pump laser, cavity mode and FP mode frequencies are tuned to produce and pass a single signal-idler mode pair within the 794.7 nm D_1 line of atomic Rb, with frequency difference $\omega_-^0 = \omega_s^0 - \omega_i^0$, between the central frequencies. The measurement is performed for two values of $\omega_-^0/(2\pi)$, 250 and 165 MHz. Single-mode fibers and linear polarizers ensure good spatial and polarization matching when the signal and idler photons arrive at the BS via spatial modes A and B, respectively. BS output modes C and D are coupled into single mode fibers leading to avalanche photodiodes (APDs, Perkin Elmer SPCM-AQ4C, quantum efficiency $\approx 50\%$). A field programmable gate array (FPGA) records all APD firings with a resolution of 625 ps (sampling rate 1.6 GHz).

The two-photon state at the output of a CE-SPDC system when pumped by a cw laser of frequency ω_p is given by Eq. (1) with $\omega_{A/B} \to \omega_{s/i}$, $f \to f'$ and

$$f'(\omega_s, \omega_i) = \delta(\omega_p - \omega_i - \omega_s) F(\omega_s, \omega_i) \times \mathcal{A}(\omega_s, \gamma, \omega_s^0, \mathrm{FSR}_s) \mathcal{A}(\omega_i, \gamma, \omega_i^0, \mathrm{FSR}_i), \quad (3)$$

where $F(\omega_s, \omega_i)$ is the collinear phase-matching amplitude for the SPDC process and the delta function imposes energy conservation [33]. For $\nu \in s, i$,

$$\mathcal{A}(\omega_\nu, \gamma, \omega_\nu^0, \mathrm{FSR}_\nu) = \sum_m \frac{\sqrt{\gamma/2\pi}}{\gamma/2 + i(\omega_\nu^0 + m\mathrm{FSR}_\nu - \omega_\nu)}, \quad (4)$$

where the mode index m is summed over positive and negative integers. In practice, the summations can be truncated to cover only those values for which $F(\omega_s, \omega_i)$ is significant.

When FP cavities are used to filter the multimode CE-SPDC output, the two-photon JSA after the filters is

$$f(\omega_s, \omega_i) = f'(\omega_s, \omega_i) \mathcal{A}(\omega_s, \gamma_f, \omega_{f_s}^0, \mathrm{FSR}_f) \times \mathcal{A}(\omega_i, \gamma_f, \omega_{f_i}^0, \mathrm{FSR}_f). \quad (5)$$

If the FP filters are tuned to the preferred CE-SPDC output modes as described above, the filters' index frequencies coincide with those of the CE-SPDC cavity, i.e., $\omega_{f_\nu}^0 = \omega_\nu^0$. In this case, the JSA for our FP and CE-SPDC linewidths and FSRs, is well approximated by a Lorentzian each for the signal and idler

$$\begin{aligned} f(\omega_s, \omega_i) &\propto \delta(\omega_p - \omega_+) \prod_{\nu \in \{s,i\}} \frac{\sqrt{\gamma/2\pi}}{\gamma/2 + i(\omega_\nu^0 - \omega_\nu)} \\ &\propto \delta(\omega_p - \omega_+) \frac{1}{\gamma^2 + (\omega_s^0 - \omega_i^0 - \omega_-)^2} \\ &\equiv \delta(\omega_p - \omega_+) g(\omega_-). \end{aligned} \quad (6)$$

When inserted into Eq. (2), we find

$$G_{C,C/D}^{(2)}(t, t') \propto \left| \int d\omega_- g(\omega_-) \mathrm{osc}(\omega_- t_-/2) \right|^2. \quad (7)$$

Figure 3(a) shows the observed and predicted $G_{C,D}^{(2)}$ for a frequency difference of $\omega_-^0 = 2\pi \times 250$ MHz between the signal and idler modes. In accordance with the theory, the results show a clear oscillation with period 4 ns, the inverse of 250 MHz. The visibility of the interference is 82%, which is greater than the classical limit of 50% [30], attests to the fact that the interference was produced by nonclassical states. The predicted $G_{C,D}^{(2)}$, calculated with

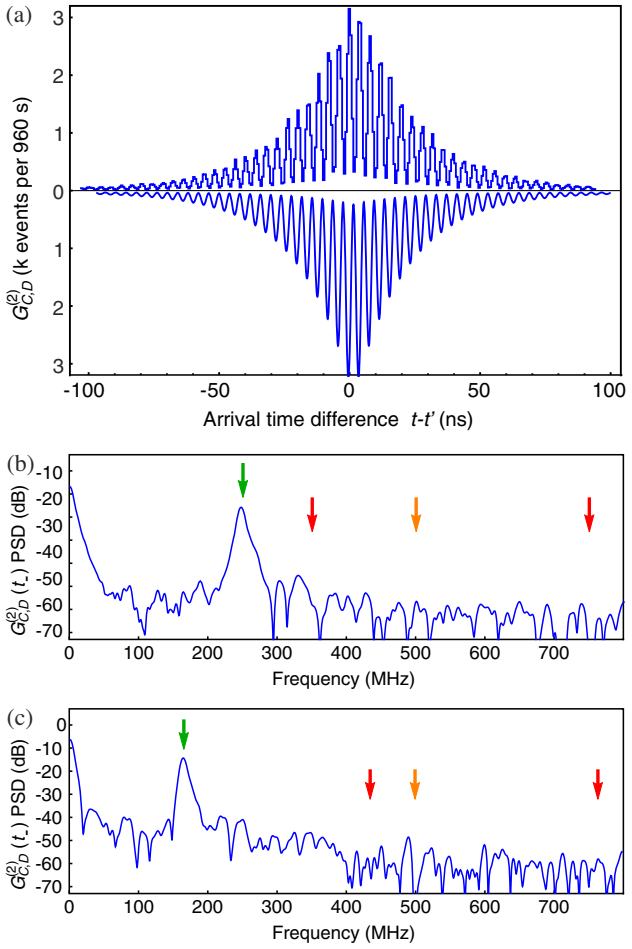

FIG. 3. Observed and predicted $G^{(2)}_{C,D}$ cross-correlation and spectral analysis. (a) (upper curve) Histogram of recorded arrival time differences with 625 ps time bins, for $\omega^0_- = 2\pi \times 250$ MHz. (lower curve) Predicted $G^{(2)}_{C,D}$ with factors chosen manually such that the amplitude and visibility match the experimental results. (b) and (c) Power spectral density (PSD) of $G^{(2)}_{C,D}(t_-)$ computed from observed histogram for $\omega^0_- = 2\pi \times 250$ and $2\pi \times 165$ MHz, respectively. The expected beat notes are clearly seen at 250 and 165 MHz (green arrows). Locations at which spectral contamination might be expected are indicated with red and orange arrows. The contamination is at least 25 dB below the power level of the desired beat note.

$\gamma = 2\pi \times 7.6$ MHz, agrees with the observed fringe period and also with the decay rate of the exponential envelope. Equation (6) implies a FWHM bandwidth of $\gamma\sqrt{\sqrt{2}-1} = 2\pi \times 4.9$ MHz for signal, idler, and difference frequency [33]. The AHC measurement was repeated for a signal-idler frequency difference of 165 MHz, and thus an oscillation period ≈ 6 ns in $G^{(2)}_{C,D}$.

The power spectra of the observed $G^{(2)}_{C,D}$ for $\omega^0_-/2\pi$ of 250 and 165 MHz are shown in Figs. 3(b) and 3(c), respectively. Each shows a peak at dc and a Lorentzian peak at the corresponding ω^0_-, of the same width and center frequency as the Lorentzian in the JSI computed from Eq. (6) [24]. The resolution of these spectra is inversely proportional to the range of $t - t'$, which can extend to the full acquisition time. In practice, the resolution is much finer than any spectral feature. The spectral range, i.e., the largest observable difference frequency, is set by the time resolution of the detection. With few-ps detection [34], a difference-frequency range of ~100 GHz can be achieved [24].

Inefficient extinction of neighbouring CE-SPDC modes by the FP filter would manifest as additional signals in the PSD besides one at the expected ω^0_-. In Fig. 3(b), peaks at 750 and/or 350 MHz (aliased down from 1250 MHz due to the sampling rate of the FPGA) would indicate leakage of mode pairs with $\omega_-/2\pi = 250$ MHz $\pm$ 2FSR (red arrows). A peak at 500 MHz (the FSR for both signal and idler) might also be expected, but is not seen (orange arrow). Similarly, leakage would produce peaks at 765 and 435 MHz (red arrows), and again 500 MHz (orange arrow) in Fig. 3(c). We thus conclude that the FP cavity filtering succeeds in blocking contributions from neighboring CE-SPDC modes and that the combined CE-SPDC and filter system emits on one pair of CE-SPDC cavity modes.

Measurement of $G^{(2)}_{C,C}$, showing the temporal GM effect, is shown in Fig. 4 for $\omega^0_- = 2\pi \times 250$ MHz. Typically SPDC $G^{(2)}$ autocorrelations require a BS and two detectors, in order to record photon pairs that arrive spaced by less than a detector's dead time, here ≈ 40 ns. For narrow-band photon pairs, however, it is possible to acquire the autocorrelation with just one detector, as we do here. The predicted oscillation with a period of 4 ns is clearly observed. The temporal GM effect thus offers a simple way to characterize relative frequencies with a single detector. Frequency-shifting of one input photon through nonlinear-optical frequency conversion [35], would allow AHC to measure spectra with difference frequencies outside the detection electronics' bandwidth.

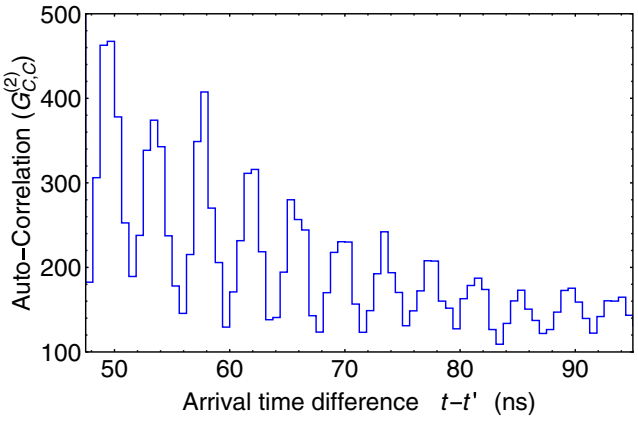

FIG. 4. Temporal GM effect. Graph shows the un-normalized autocorrelation detected in detector C ($G^{(2)}_{C,C}$) after the BS. The oscillations corresponding to the inverse frequency difference for $\omega^0_- = 2\pi \times 250$ MHz.

We have demonstrated a new technique to quantify the frequency correlations of narrow-band photon pairs and applied it to measure the spectral content of a filtered, cavity-enhanced parametric down-conversion source at the Rb D_1 line with ≈ 5 MHz optical bandwidth. By interfering the photons on a BS and performing Fourier analysis on the temporal auto- and cross-correlations, AHC directly measures the beat-note spectrum with the spectral resolution limited only by the acquisition time. The technique is simple to implement with one detector via the temporal Ghosh-Mandel effect, or with two detectors via the nondegenerate Hong-Ou-Mandel effect. It is well suited to characterize narrow-band photon sources for interaction with atoms and ions, which typically require bandwidths below 10 MHz. The technique may be especially valuable in quantum networking, computing, and simulation with mixed photon-atom systems.

We thank Dr. Robert Sewell, Samyobrata Mukherjee, and Natália Alves for feedback on the manuscript. This project was supported by H2020 Future and Emerging Technologies Quantum Technologies Flagship project QRANGE (Grant Agreement No. 820405); Spanish MINECO projects OCARINA (Grant No. PGC2018-097056-B-I00), Q-CLOCKS (Grant No. PCI2018-092973), and the Severo Ochoa program (Grant No. SEV-2015-0522); Generalitat de Catalunya through the CERCA program; Agència de Gestió d'Ajuts Universitaris i de Recerca Grant No. 2017-SGR-1354; Secretaria d'Universitats i Recerca del Departament d'Empresa i Coneixement de la Generalitat de Catalunya, co-funded by the European Union Regional Development Fund within the ERDF Operational Program of Catalunya (project QuantumCat, ref. 001-P-001644); Fundació Privada Cellex; Fundació Mir-Puig; European Union's H2020 Marie Skłodowska-Curie Actions (Grant Agreement No. 665884). National Science Centre, Poland (2018/28/T/ST2/00275 and 2019/34/E/ST2/00440).

*vindhiya.prakash@icfo.eu
†morgan.mitchell@icfo.es

[1] C. Couteau, Contemp. Phys. **59**, 291 (2018).
[2] C. Reimer, S. Sciara, P. Roztocki, M. Islam, L. Romero Cortés, Y. Zhang, B. Fischer, S. Loranger, R. Kashyap, A. Cino, S. T. Chu, B. E. Little, D. J. Moss, L. Caspani, W. J. Munro, J. Azaña, M. Kues, and R. Morandotti, Nat. Phys. **15**, 148 (2019).
[3] O. Pfister, J. Phys. B **53**, 012001 (2019).
[4] T. Gerrits, F. Marsili, V. B. Verma, L. K. Shalm, M. Shaw, R. P. Mirin, and S. W. Nam, Phys. Rev. A **91**, 013830 (2015).
[5] Y.-H. Kim and W. P. Grice, Opt. Lett. **30**, 908 (2005).
[6] K. Zielnicki, K. Garay-Palmett, D. Cruz-Delgado, H. Cruz-Ramirez, M. F. O'Boyle, B. Fang, V. O. Lorenz, A. B. U'Ren, and P. G. Kwiat, J. Mod. Opt. **65**, 1141 (2018).
[7] W. Wasilewski, P. Wasylczyk, P. Kolenderski, K. Banaszek, and C. Radzewicz, Opt. Lett. **31**, 1130 (2006).
[8] S. Mittal, V. V. Orre, A. Restelli, R. Salem, E. A. Goldschmidt, and M. Hafezi, Phys. Rev. A **96**, 043807 (2017).
[9] C. K. Hong, Z. Y. Ou, and L. Mandel, Phys. Rev. Lett. **59**, 2044 (1987).
[10] T. Gerrits, M. J. Stevens, B. Baek, B. Calkins, A. Lita, S. Glancy, E. Knill, S. W. Nam, R. P. Mirin, R. H. Hadfield, R. S. Bennink, W. P. Grice, S. Dorenbos, T. Zijlstra, T. Klapwijk, and V. Zwiller, Opt. Express **19**, 24434 (2011).
[11] S. Wang, C.-X. Liu, J. Li, and Q. Wang, Sci. Rep. **9**, 3854 (2019).
[12] V. Thiel, A. O. C. Davis, K. Sun, P. D'Ornellas, X.-M. Jin, and B. J. Smith, Opt. Express **28**, 19315 (2020).
[13] O. Slattery, L. Ma, K. Zong, and X. Tang, J. Res. Natl. Inst. Stand. Technol. **124**, 124019 (2019).
[14] E. Distante, P. Farrera, A. Padrón-Brito, D. Paredes-Barato, G. Heinze, and H. de Riedmatten, Nat. Commun. **8**, 14072 (2017).
[15] A. Seri, A. Lenhard, D. Rieländer, M. Gündoğan, P. M. Ledingham, M. Mazzera, and H. de Riedmatten, Phys. Rev. X **7**, 021028 (2017).
[16] A. Asenjo-Garcia, M. Moreno-Cardoner, A. Albrecht, H. J. Kimble, and D. E. Chang, Phys. Rev. X **7**, 031024 (2017).
[17] J. Perczel, J. Borregaard, D. E. Chang, H. Pichler, S. F. Yelin, P. Zoller, and M. D. Lukin, Phys. Rev. Lett. **119**, 023603 (2017).
[18] J. Rui, D. Wei, A. Rubio-Abadal, S. Hollerith, J. Zeiher, D. M. Stamper-Kurn, C. Gross, and I. Bloch, Nature (London) **583**, 369 (2020).
[19] S. J. Masson and A. Asenjo-Garcia, Phys. Rev. Research **2**, 043213 (2020).
[20] I. H. Deutsch, R. Y. Chiao, and J. C. Garrison, Phys. Rev. Lett. **69**, 3627 (1992).
[21] Y. Ke, J. Zhong, A. V. Poshakinskiy, Y. S. Kivshar, A. N. Poddubny, and C. Lee, Phys. Rev. Research **2**, 033190 (2020).
[22] V. Prakash, L. C. Bianchet, M. T. Cuairan, P. Gomez, N. Bruno, and M. W. Mitchell, Opt. Express **27**, 38463 (2019).
[23] F. Monteiro, A. Martin, B. Sanguinetti, H. Zbinden, and R. T. Thew, Opt. Express **22**, 4371 (2014).
[24] See Supplemental Material at http://link.aps.org/supplemental/10.1103/PhysRevLett.127.043601 for application of AHC to heralded pure state characterization, calculations relating the power spectral density of the AHC $G^{(2)}$ to the JSA, discussions related to the resolution of AHC, and first order interference effects from single photon states.
[25] M. Liscidini and J. E. Sipe, Phys. Rev. Lett. **111**, 193602 (2013).
[26] T. Jeong and H. S. Moon, Opt. Lett. **45**, 2668 (2020).
[27] I. Jizan, B. Bell, L. G. Helt, A. C. Bedoya, C. Xiong, and B. J. Eggleton, Opt. Lett. **41**, 4803 (2016).
[28] Z. Y. Ou and L. Mandel, Phys. Rev. Lett. **61**, 54 (1988).
[29] R.-B. Jin and R. Shimizu, Optica **5**, 93 (2018).

[30] R. Ghosh and L. Mandel, Phys. Rev. Lett. **59**, 1903 (1987).
[31] Y. Okawa, F. Omura, Y. Yasutake, and S. Fukatsu, Opt. Express **25**, 20156 (2017).
[32] A. M. Brańczyk, T. C. Ralph, W. Helwig, and C. Silberhorn, New J. Phys. **12**, 063001 (2010).
[33] M. Scholz, L. Koch, and O. Benson, Opt. Commun. **282**, 3518 (2009).
[34] B. Korzh *et al.*, Nat. Photonics **14**, 250 (2020).
[35] N. Maring, D. Lago-Rivera, A. Lenhard, G. Heinze, and H. de Riedmatten, Optica **5**, 507 (2018).